

# Surface Passivation of TiO<sub>2</sub> Nanowires Using a Facile Precursor-Treatment Approach for Photoelectrochemical Water Oxidation

Ying-Chih Pu,<sup>†,‡</sup> Yichuan Ling,<sup>‡</sup> Kao-Der Chang,<sup>§</sup> Chia-Ming Liu,<sup>||</sup> Jin Z. Zhang,<sup>‡</sup> Yung-Jung Hsu,<sup>\*,†</sup> and Yat Li<sup>\*,‡</sup>

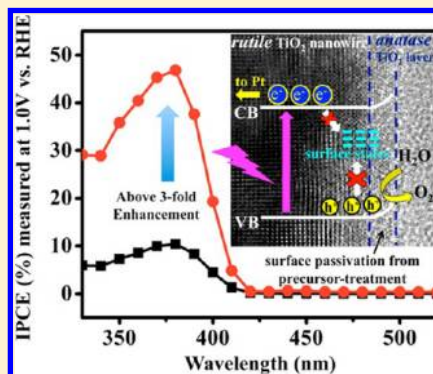
<sup>†</sup>Department of Materials Science and Engineering, National Chiao Tung University, 1001 University Road, Hsinchu 30010, Taiwan, ROC

<sup>‡</sup>Department of Chemistry and Biochemistry, University of California—Santa Cruz, Santa Cruz, California 95064, United States

<sup>§</sup>Mechanical and Systems Research Laboratories and <sup>||</sup>Green Energy and Environment Research Laboratories, Industrial Technology Research Institute, 195, Section 4, Chung Hsing Road, Chutung, Hsinchu 31040, Taiwan, ROC

## Supporting Information

**ABSTRACT:** We developed a facile precursor-treatment approach for effective surface passivation of rutile TiO<sub>2</sub> nanowire photoanode to improve its performance in photoelectrochemical (PEC) water oxidation. The approach was demonstrated by treating rutile TiO<sub>2</sub> nanowires with titanium precursor solutions (TiCl<sub>4</sub>, Ti(OBu)<sub>4</sub>, or Ti(OiP)<sub>4</sub>) followed by a postannealing process, which resulted in the additional deposition of anatase TiO<sub>2</sub> layer on the nanowire surface. Compared to pristine TiO<sub>2</sub>, all the precursor-treated TiO<sub>2</sub> nanowire electrodes exhibited a significantly enhanced photocurrent density under white light illumination. Among the three precursor-treated samples, Ti(OBu)<sub>4</sub>-treated TiO<sub>2</sub> nanowires achieved the largest enhancement of photocurrent generation, which is approximately a 3-fold increase over pristine TiO<sub>2</sub>. Monochromatic incident photon-to-electron conversion efficiency (IPCE) measurements showed that the improvement of PEC performance was dominated by the enhanced photoactivity of TiO<sub>2</sub> in the UV region. The photovoltage and electrochemical impedance spectroscopy (EIS) measurements showed that the enhanced photoactivity can be attributed to the improved charge transfer as a result of effective surface state passivation. This work demonstrates a facile, low-cost, and efficient method for preparing highly photoactive TiO<sub>2</sub> nanowire electrodes for PEC water oxidation. This approach could also potentially be used for other photoconversion applications, such as TiO<sub>2</sub> based dye-sensitized solar cells, as well as photocatalytic systems.



## INTRODUCTION

Artificial photosynthesis for solar fuel production is a green and effective solution to development of renewable and sustainable carbon-free energy sources.<sup>1–4</sup> Particularly, photoelectrochemical (PEC) cells provide a promising way for practically converting solar energy to storable clean fuels such as hydrogen. Titanium dioxide (TiO<sub>2</sub>) has been extensively utilized as photoanode in PEC water splitting because of its favorable band edge position, high chemical stability, and relatively low cost.<sup>5–16</sup> Under light illumination, the photo-generated holes at the valence band of TiO<sub>2</sub> will diffuse to the TiO<sub>2</sub> surface and oxidize water,<sup>17</sup> producing O<sub>2</sub>. Meanwhile, the photoexcited electrons in the conduction band of TiO<sub>2</sub> can transfer to a (photo)cathode, reducing protons to generate H<sub>2</sub>. The structural and surface engineering of TiO<sub>2</sub> photoanode is crucial to the PEC performance because charge carriers may be trapped and recombined at the surface states before they can reach the TiO<sub>2</sub> surface for further utilization.<sup>18</sup> Nanostructures with unique morphology have demonstrated desirable properties for use as highly active photoanode. For example, one-dimensional architectures, such as nanowire or nanotube arrays,

have proven to be superior photoanode in PEC water splitting because the photoinduced charge carriers can easily transport to the structure surface along the radial direction.<sup>1,19–22</sup>

Although single-crystalline TiO<sub>2</sub> nanowires have a high electron mobility,<sup>23</sup> the photogenerated holes can be easily captured by the surface states and cause significant electron–hole recombination.<sup>18</sup> Atomic layer deposition (ALD) has been proved to be a powerful technique for surface state passivation to decrease trap state-mediated charge recombination.<sup>24–26</sup> For example, Hwang et al. demonstrated that an ALD coated TiO<sub>2</sub> shell on TiO<sub>2</sub> nanowires can increase the photocurrent by approximately 1.5 times. This improvement was attributed to the effective surface passivation of the surface states achieved by the epitaxial ALD deposition of TiO<sub>2</sub>.<sup>24</sup> Similarly, Paracchino's study showed that the stability of p-Cu<sub>2</sub>O photocathode can be substantially improved with the ALD coating of TiO<sub>2</sub>, which prevents the self-reduction of Cu<sub>2</sub>O.<sup>25</sup> Moreover, the ALD

Received: April 27, 2014

Revised: June 10, 2014

Published: June 13, 2014

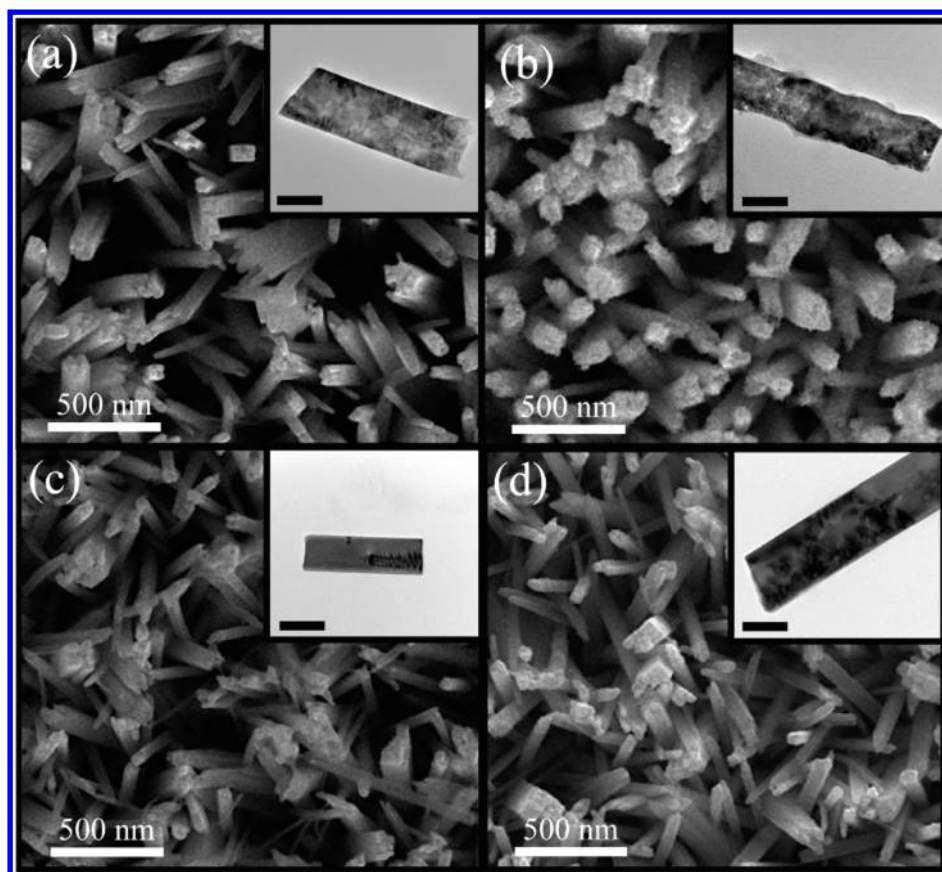


**Figure 1.** SEM images of (a) pristine  $\text{TiO}_2$ , (b)  $\text{TiO}_2$ -TCL, (c)  $\text{TiO}_2$ -TIP, and (d)  $\text{TiO}_2$ -TBU nanowire arrays. Insets show the corresponding TEM images of these samples. Scale bars in insets are 50 nm.

growth of p–n  $\text{Fe}_2\text{O}_3$  has been shown to exhibit a low turn-on voltage and superior photocatalytic water splitting performance in comparison to n- $\text{Fe}_2\text{O}_3$ . This enhancement was ascribed to the building of internal field by the p–n junction that reduces charge trapping and results in better charge separation and improved carrier utilization.<sup>26</sup> However, the powerful ALD technique is expensive to set up and requires hundreds of runs using layer-by-layer deposition that is time-intensive. Therefore, development of a facile wet-chemistry-based method to achieve effective surface passivation is imperative for  $\text{TiO}_2$  electrodes. We hypothesize that the  $\text{TiO}_2$  photoanodes can be passivated by a secondary growth of  $\text{TiO}_2$  film using a technologically viable approach like hydrothermal process or sol–gel method.

In this work, we introduced a facile precursor-treatment approach to modify the surface of rutile  $\text{TiO}_2$  nanowire photoanode with anatase shell and investigated its influence on the PEC water oxidation performance. Three different titanium precursors, including titanium tetrachloride ( $\text{TiCl}_4$ ), titanium isopropoxide ( $\text{Ti}(\text{OiP})_4$ ), and titanium *n*-butoxide ( $\text{Ti}(\text{OBu})_4$ ), were employed to form anatase shells. Electron microscopy characterizations showed that a uniform layer of anatase  $\text{TiO}_2$  film was deposited on the rutile  $\text{TiO}_2$  nanowires after the precursor-treatment. Comparative studies demonstrated that the photocurrent of  $\text{TiO}_2$  nanowires for PEC water oxidation can be enhanced 3-fold with the treatment of  $\text{Ti}(\text{OBu})_4$ . The photovoltage measurements showed that the enhanced photoactivity of precursor-treated  $\text{TiO}_2$  was attributable to effective surface state passivation. Furthermore, the electrochemical impedance spectroscopy (EIS) studies suggested that the significantly improved PEC performance of precursor-treated

$\text{TiO}_2$  nanowires originates from the improved charge transfer at the  $\text{TiO}_2$ /electrolyte interface, as a result of effective surface passivation.

## EXPERIMENTAL SECTION

**Preparation of  $\text{TiO}_2$  Nanowire Arrays.** Rutile  $\text{TiO}_2$  nanowire arrays were grown on fluorine-doped tin oxide (FTO) glass substrates using a hydrothermal method reported elsewhere.<sup>6</sup> Concentrated hydrochloric acid (15 mL) was diluted with 15 mL of deionized (DI) water and was then mixed with 0.5 mL of titanium *n*-butoxide in a 100 mL beaker. The resulting clear solution was transferred to a Teflon-lined stainless steel autoclave (40 mL volume), where a clean FTO glass substrate was submerged into the solution. The sealed autoclave was heated in an electric oven at 150 °C for 5 h and then slowly cooled to room temperature. A white  $\text{TiO}_2$  nanowire film was uniformly coated on the FTO glass substrate after cooling. The sample was thoroughly washed with DI water and then air-dried. Finally, the sample was annealed in air at 550 °C on for 3 h to improve the crystallinity of  $\text{TiO}_2$  nanowires.

**Precursor-Treatment on  $\text{TiO}_2$  Nanowires.** Precursor-treatment of the  $\text{TiO}_2$  nanowires was performed by using titanium tetrachloride ( $\text{TiCl}_4$ ), titanium isopropoxide ( $\text{Ti}(\text{OiP})_4$ ), and titanium *n*-butoxide ( $\text{Ti}(\text{OBu})_4$ ) as precursors. First, the titanium precursors were dissolved in an aqueous 2 M HCl solution to form the 20% precursor sol solution. To conduct the precursor-treatment,  $\text{TiO}_2$  nanowire arrays grown on FTO substrates were immersed in 10 mL of an aqueous HCl solution (0.025 M) containing 50  $\mu\text{L}$  of the precursor

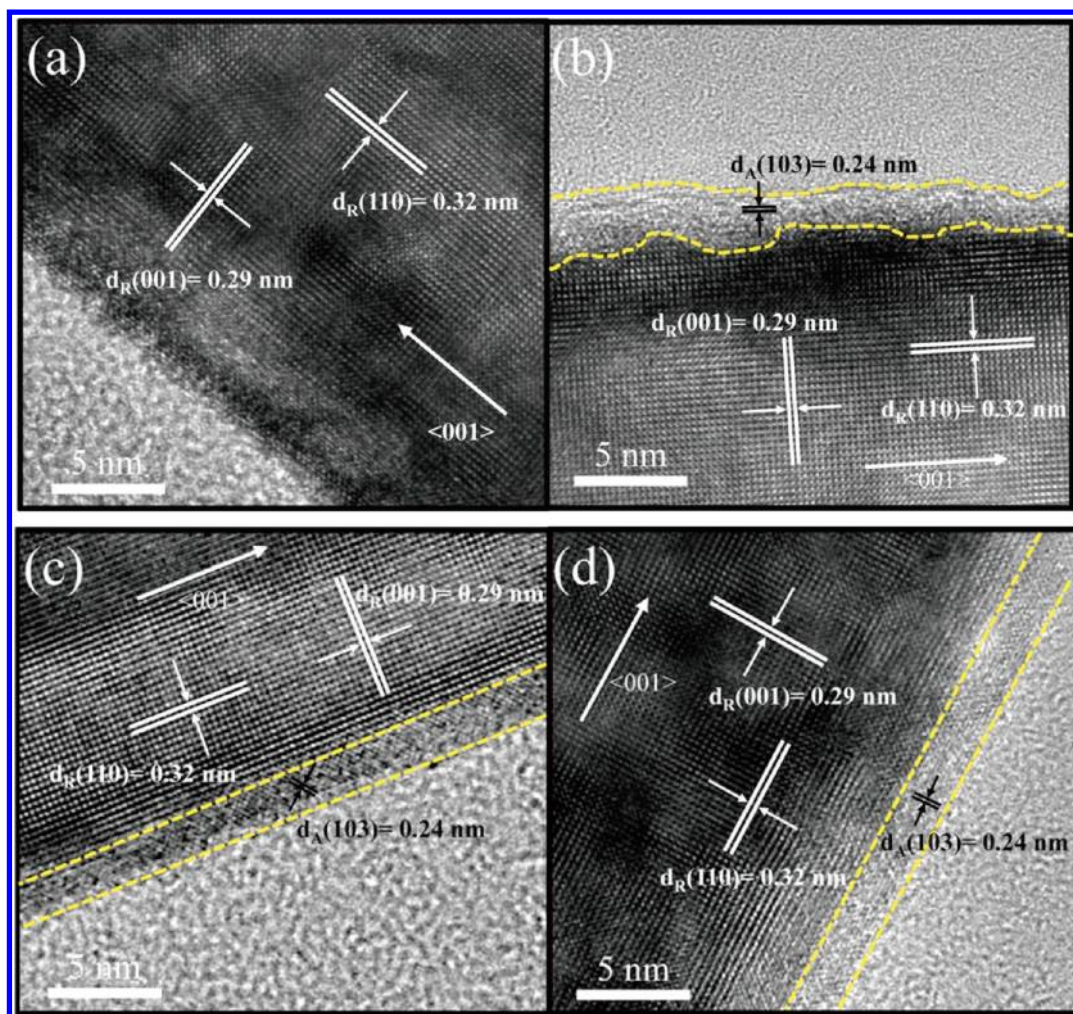


**Figure 2.** HR-TEM images of (a) pristine  $\text{TiO}_2$ , (b)  $\text{TiO}_2$ -TCL, (c)  $\text{TiO}_2$ -TIP, and (d)  $\text{TiO}_2$ -TBU nanowire arrays. In (b)–(d), the A- $\text{TiO}_2$  layers are highlighted with the inserted dashed lines.

solution in a 20 mL glass vial. The sealed glass vial was heated in an electric oven at  $90^\circ\text{C}$  for 1 h and then slowly cooled to room temperature. The sample was thoroughly washed with DI water and then air-dried. Finally, the sample was annealed in air at  $350^\circ\text{C}$  on a hot plate (Corning PC-420D, panel temperature was set at  $550^\circ\text{C}$ ) for 1 h. In this work, different amounts of  $\text{Ti}(\text{O}i\text{Bu})_4$  solutions (12.5, 25, 50, and 75  $\mu\text{L}$ ) were employed in the TBU-treatment to investigate the quantitative effect on the photoactivity of  $\text{TiO}_2$  nanowires. The thus-obtained samples were respectively denoted as  $\text{TiO}_2$ -TBU-12.5,  $\text{TiO}_2$ -TBU-25,  $\text{TiO}_2$ -TBU-50, and  $\text{TiO}_2$ -TBU-75.

**Characterization of Materials.** Absorption spectra were recorded using a Hitachi U-3900H spectrophotometer at room temperature under ambient atmosphere. Scanning electron microscopy (SEM) images were collected with a field-emission SEM (Hitachi S-4800 II). Transmission electron microscopy (TEM) images were collected using a FEI monochromated F20 UT Technai TEM/STEM operated at 200 kV. X-ray diffraction (XRD) spectra were collected with Rigaku Americas Miniflex Plus powder diffractometer. Raman spectroscopy measurements were carried out on a Nicolet Almega XR dispersive Raman spectrometer (laser wavelength of 780 nm).  $\text{N}3/\text{TiO}_2$  desorption experiments were performed using the following process. First, the prepared  $\text{TiO}_2$  samples were immersed in a 0.3 M ethanolic solution of *cis*-bis(isothiocyanato)bis(2,2'-

bipyridyl-4,4'-dicarboxylato)ruthenium(II) (N3, Fisher) for 24 h, then washed with ethanol and air-dried. After the  $\text{N}3/\text{TiO}_2$  samples were dry, they were immersed in a solution containing 0.5 mL of ethanol and 0.5 mL of a NaOH aqueous solution (0.2 M) for 1 h to desorb the N3 dye.

**Photoelectrochemical Measurements.** The pristine  $\text{TiO}_2$  and precursor-treated  $\text{TiO}_2$  nanowire arrays were fabricated into photoanodes by soldering a copper wire onto a bare part of the FTO substrate. The substrate edges and the metal contact region were sealed with insulating epoxy resin. The working electrode area is in the range of 0.2–0.25  $\text{cm}^2$ . A 1 M KOH aqueous solution (pH 13.6) was used as an electrolyte for PEC measurements. Linear sweeps and  $I-t$  scans were measured by a CHI 660D electrochemical station using Ag/AgCl as a reference electrode and Pt wire as a counter electrode, under simulated sunlight using a 150 W xenon lamp (Newport 6255) coupled with an AM 1.5 global filter (Newport 81094). Incident-photon-to-current conversion efficiencies (IPCE) were collected by a Solartron 1280B electrochemical station with a solar simulator (Newport 69920, 1000 W xenon lamp) coupled with an infrared water filter (Oriel 6127) and aligned monochromator (Oriel Cornerstone 130 1/8 m). The EIS measurement was carried out in the frequency range from 100 kHz to 50 mHz at the open-circuit

potential of 0.2 V. The fitting of EIS data was performed by using the Z-view software.

## RESULTS AND DISCUSSION

TiO<sub>2</sub> nanowire arrays were synthesized on fluorine-doped tin oxide (FTO) glass substrates using a hydrothermal method reported elsewhere.<sup>6</sup> The prepared TiO<sub>2</sub> nanowires were treated with different titanium precursors by immersing them in the respective solutions at 90 °C for 1 h. The samples were then annealed in air at 350 °C on a hot plate for 1 h to increase the crystallinity. The thus-obtained TiO<sub>2</sub> nanowires were denoted as “TiO<sub>2</sub>-TCL” (treated with TiCl<sub>4</sub>), “TiO<sub>2</sub>-TIP” (treated with Ti(OiP)<sub>4</sub>), and “TiO<sub>2</sub>-TBU” (treated with Ti(OBu)<sub>4</sub>). The scanning electron microscopy (SEM) images shown in Figure 1 demonstrated that the morphology of the three precursor-treated nanowires is similar to that of the pristine TiO<sub>2</sub> nanowires. The surface characteristics of the samples were further characterized with transmission electron microscopy (TEM). As shown in the insets of Figure 1, both TiO<sub>2</sub>-TIP and TiO<sub>2</sub>-TBU nanowires have a smooth surface similar to pristine TiO<sub>2</sub>. In contrast, TiO<sub>2</sub>-TCL nanowires possess a rough surface on which a number of small particles were attached.

High-resolution TEM (HR-TEM) analysis was performed to examine the detailed structure of TiO<sub>2</sub> nanowires upon the precursor-treatment. As shown in Figure 2a, pristine TiO<sub>2</sub> nanowires exhibited a well-resolved crystalline structure with two distinct sets of lattice fringes that can be assigned to rutile TiO<sub>2</sub> (R-TiO<sub>2</sub>). Compared to pristine TiO<sub>2</sub> nanowires that presented a homogeneous surface, all the precursor-treated samples showed atomically abrupt interfaces at the surface, suggesting that an additional layer of TiO<sub>2</sub> was deposited on the nanowire surface during the precursor-treatment process. The crystallographic structure of the deposited shells was identified as anatase TiO<sub>2</sub> (A-TiO<sub>2</sub>) by characterizing the lattice fringes. TiO<sub>2</sub>-TCL nanowires have a rough interface between the R-TiO<sub>2</sub> nanowires and A-TiO<sub>2</sub> shell, as revealed in Figure 2b. The thickness of the A-TiO<sub>2</sub> shell is approximately 1.7–2.5 nm. On the contrary, a uniform and epitaxial A-TiO<sub>2</sub> layer was found to form on the surface of TiO<sub>2</sub>-TIP and TiO<sub>2</sub>-TBU nanowires, as shown in Figure 2c and Figure 2d. The A-TiO<sub>2</sub> shell thickness was approximately 2 nm. In order to further confirm the crystallographic structure of TiO<sub>2</sub> shell, we performed the XRD and Raman characterizations for bare TiO<sub>2</sub> and precursor-treated TiO<sub>2</sub> samples. Both of the XRD and Raman analysis results indicated that the pristine TiO<sub>2</sub> and precursor-treated TiO<sub>2</sub> were rutile crystallite phase (Figure S1a and S1b in Supporting Information).<sup>8,27</sup> Because of the considerably small thickness, the signal contribution from the coated shell may be imperceptible in XRD and Raman measurements. In this regard, we used an indirect method to determine the structure of coated shell on TiO<sub>2</sub>. During the precursor-treatment process, the particle suspensions are formed in the solution together with the shell coating on the TiO<sub>2</sub> nanowires. We annealed these particle suspensions in air at 350 °C, as we did for the core–shell nanowire samples. The XRD spectra (Figure S1c) show that the particle suspensions collected from three different precursor-treatment processes are all anatase TiO<sub>2</sub>. These XRD results together with the TEM images suggest that the crystal phase of TiO<sub>2</sub> shell layers from the precursor treatment should be anatase phase. In addition, the rough surface and interface observed for TiO<sub>2</sub>-TCL nanowires suggest that an etching process was possibly involved

during the TiCl<sub>4</sub>-treatment. It has been reported that Cl<sup>−</sup> ions can easily adsorb on the (110) plane of R-TiO<sub>2</sub> and guide the anisotropic crystal growth to form TiO<sub>2</sub> nanorods because of the abundant five-coordinated Ti<sup>4+</sup> atoms and oxygen vacancies.<sup>28,29</sup> Also, it has been demonstrated that thick R-TiO<sub>2</sub> nanowires could be split into secondary nanorods because of the HCl etching effect.<sup>30,31</sup> We postulate that the high concentration of Cl<sup>−</sup> in the TiCl<sub>4</sub>-treatment operation would enable Cl<sup>−</sup> adsorption on the (110) plane of the R-TiO<sub>2</sub> nanowires, which could pose an effect analogous to HCl etching to form a rough R-TiO<sub>2</sub>/A-TiO<sub>2</sub> interface. The distribution of surface roughness on the lateral (110) plane of R-TiO<sub>2</sub> nanowires may support the above argument.

The effect of the A-TiO<sub>2</sub> deposition from the precursor-treatment process on the PEC properties of TiO<sub>2</sub> nanowire photoanodes was studied in a three-electrode cell with a Pt wire as the counter electrode and Ag/AgCl as the reference electrode. Figure 3a shows a set of linear sweep voltammograms of pristine TiO<sub>2</sub> and precursor-treated TiO<sub>2</sub> nanowire electrodes recorded in 1 M KOH electrolyte in the dark and under white light illumination (AM 1.5G, 100 mW/cm<sup>2</sup>). The values of potential are presented with respect to reversible hydrogen electrode (RHE), which were determined by the Nernst equation:  $RHE = V_{vs Ag/AgCl} + E^{\circ}_{Ag/AgCl} + 0.059 \times pH = V_{vs Ag/AgCl} + 1.0 V$ , where  $E^{\circ}_{Ag/AgCl}$  is +0.1976 V at 25 °C (in 1.0 M KOH).<sup>32</sup> As shown in Figure 3a, the dark scans collected in the potential range between 0 and 1.5 V vs RHE displayed a negligible background current of  $\sim 10^{-8}$  A/cm<sup>2</sup>. Upon light illumination, pristine TiO<sub>2</sub> and all precursor-treated TiO<sub>2</sub> nanowire electrodes showed pronounced photoresponse. Significantly, the precursor-treated TiO<sub>2</sub> nanowire electrodes showed higher photocurrent densities than pristine TiO<sub>2</sub>. Among all the precursor-treated TiO<sub>2</sub> nanowire electrodes examined, the TiO<sub>2</sub>-TBU electrode achieved the highest photocurrent density of 1.32 mA/cm<sup>2</sup> at 1.23 V vs RHE, which is almost 3 times higher than that of pristine TiO<sub>2</sub> (0.45 mA/cm<sup>2</sup>) obtained at the same potential. Furthermore, the performance of surface passivated TiO<sub>2</sub>-TBU is comparable to the best values reported for TiO<sub>2</sub> nanowires for photoelectrochemical water oxidation.<sup>6,8,9,24,32,33</sup> These results confirmed the positive role of precursor-treatment operation in enhancing the photoactivity of TiO<sub>2</sub> nanowires toward PEC water oxidation. This effect was further studied quantitatively. As shown in Figure S2 (Supporting Information), an optimal precursor amount for enhancing the photocurrent density of TiO<sub>2</sub> nanowire electrode was noticed. Overloading the amount of Ti precursor gives rise to a thick A-TiO<sub>2</sub> layer (Figure S3, Supporting Information). The thick A-TiO<sub>2</sub> layer is polycrystalline in nature and has abundant grain boundaries that may induce new trap states to obstruct hole transfer to the electrode surface. To evaluate the stability of the precursor-treated TiO<sub>2</sub> nanowires, an amperometric  $I-t$  study was performed. The photocurrent density of TiO<sub>2</sub>-TBU was very stable under continuous illumination for over 3 h (Figure 3b). These results demonstrated that the precursor-treated nanowires exhibited remarkable photoactivity and photostability.

To further elucidate the role of precursor-treatment operation in improving the PEC performance of TiO<sub>2</sub>, we collected IPCE spectra for pristine TiO<sub>2</sub> and precursor-treated TiO<sub>2</sub> nanowire electrodes (Figure 3c). IPCE values at specific wavelengths can be determined from eq 1:<sup>34</sup>

$$IPCE = (1240I) / (\lambda J_{light}) \quad (1)$$

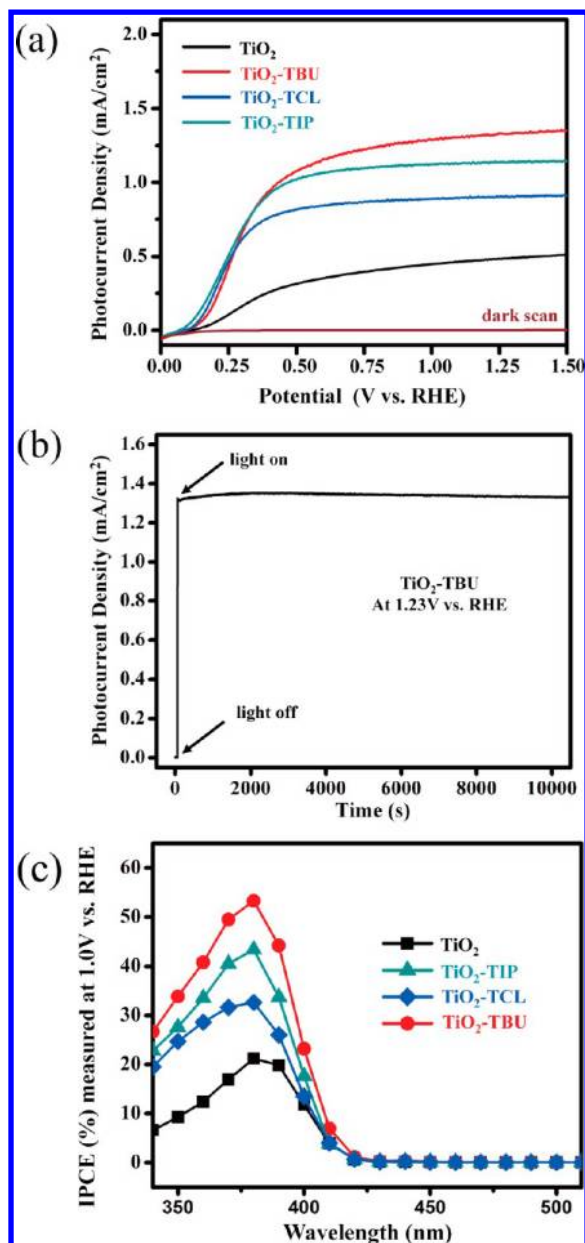


**Figure 3.** (a) Linear sweep voltammograms of pristine TiO<sub>2</sub>, TiO<sub>2</sub>-TCL, TiO<sub>2</sub>-TIP, and TiO<sub>2</sub>-TBU nanowire electrodes recorded in a 1 M KOH solution in the dark and under white light illumination (AM 1.5G, 100 mW/cm<sup>2</sup>). (b) Chronoamperometric  $I-t$  curve for TiO<sub>2</sub>-TBU collected at 1.23 V vs RHE under white light illumination. (c) IPCE plots of pristine TiO<sub>2</sub>, TiO<sub>2</sub>-TCL, TiO<sub>2</sub>-TIP, and TiO<sub>2</sub>-TBU nanowire electrodes collected at 1 V vs RHE.

where  $I$  is the measured photocurrent density,  $J_{\text{light}}$  is the measured irradiance at a specific wavelength, and  $\lambda$  is the incident light wavelength. The precursor-treated TiO<sub>2</sub> nanowires exhibited higher photoactivity than pristine TiO<sub>2</sub> nanowires, and the TiO<sub>2</sub>-TBU sample showed the largest IPCE enhancement. Significantly, the photocurrent enhancement of precursor-treated TiO<sub>2</sub> nanowires was dominated by the photoactivity of TiO<sub>2</sub> in the UV region, indicating that the precursor-treatment improved the water oxidation performance of TiO<sub>2</sub> nanowires by effectively increasing the charge collection efficiency.<sup>35,36</sup> Since A-TiO<sub>2</sub> was deposited on the surface of the precursor-treated TiO<sub>2</sub> nanowires, a possible cause for the improved charge collection efficiency could be the

band offset created at the R-TiO<sub>2</sub>/A-TiO<sub>2</sub> interface.<sup>9</sup> We excluded this possibility because the band alignment of R-TiO<sub>2</sub>/A-TiO<sub>2</sub> in the present system was not favorable for extraction of holes. Note that the thickness of the deposited A-TiO<sub>2</sub> layer is around 2 nm in the precursor-treated TiO<sub>2</sub> samples, which could cause significant quantum effect to vary the band structure of A-TiO<sub>2</sub>.<sup>37</sup> According to the effective mass approximation, a negative shift of 0.01 eV in the conduction band edge and a positive shift of 0.12 eV in the valence band edge were considered for the 2 nm thick A-TiO<sub>2</sub>.<sup>38,39</sup> Although the slightly higher conduction band edge of A-TiO<sub>2</sub> layer may facilitate the electron transport in the R-TiO<sub>2</sub> nanowires, the much more positive valence band of A-TiO<sub>2</sub> generated an energetic barrier for hole transfer from the electrode surface to the electrolyte. Because of this unfavorable band offset, one may not expect an improved PEC performance when a 2 nm thick A-TiO<sub>2</sub> layer was deposited on the R-TiO<sub>2</sub> nanowire surface. Nevertheless, the A-TiO<sub>2</sub> deposition could intrinsically improve the charge collection efficiency of R-TiO<sub>2</sub> nanowires by considering the aspect of surface state passivation. Here we suggest that effective surface passivation is responsible for the PEC performance enhancement of precursor-treated TiO<sub>2</sub> nanowires.

To prove our hypothesis, we performed photovoltage and electrochemical impedance spectroscopy (EIS) measurements to evaluate the influence of A-TiO<sub>2</sub> on the surface properties and charge transfer at interface between photoanode and electrolyte. The surface properties of TiO<sub>2</sub> photoanode can significantly affect the overall PEC performance by affecting the kinetics of water oxidation as well as the charge recombination loss at electrode surface. Specifically, the photogenerated holes of TiO<sub>2</sub> can be trapped by the surface states and recombine with electrons before they can diffuse to the surface for water oxidation.<sup>18</sup> Therefore, a high density of surface trap states will negatively affect the PEC performance of TiO<sub>2</sub>. Recent studies have demonstrated the photovoltage decay experiment as a useful method to determine the presence of surface trap states for photoanode materials.<sup>40,41</sup> Figure 4a shows the photovoltage-time ( $V-t$ ) spectra for pristine TiO<sub>2</sub> and precursor-treated TiO<sub>2</sub> nanowire electrodes. Notably, all the precursor-treated TiO<sub>2</sub> electrodes exhibited faster photovoltage decay in comparison to the pristine TiO<sub>2</sub> electrode. The decay lifetime of each of the  $V-t$  profiles can be determined by fitting them to the following biexponential function with two time constants ( $\tau_1$  and  $\tau_2$ ):

$$y(t) = A_0 + A_1 e^{-t/\tau_1} + A_2 e^{-t/\tau_2} \quad (2)$$

$$\tau_m = (\tau_1 \tau_2) / (\tau_1 + \tau_2) \quad (3)$$

where  $\tau_1$  and  $\tau_2$  are time components for band-to-band and band-to-surface states charge recombination processes,  $\tau_m$  is the harmonic mean of the decay lifetime, and the total half-life is  $\log(2\tau_m)$ . The total half-lives of pristine TiO<sub>2</sub>, TiO<sub>2</sub>-TCL, TiO<sub>2</sub>-TIP, and TiO<sub>2</sub>-TBU were estimated to be 1.25, 1.02, 0.84, and 0.72 s, respectively. The rapid decay of precursor-treated TiO<sub>2</sub> nanowire electrodes suggested that the precursor-treatment effectively removed the surface trap states of TiO<sub>2</sub> and reduced the loss of photoexcited holes via electron-hole recombination. Among the three precursor-treated TiO<sub>2</sub> electrodes, TiO<sub>2</sub>-TBU showed the fastest photovoltage decay, indicating TBU-treatment rendered TiO<sub>2</sub> nanowires the most effective surface passivation. The trend in photovoltage decay half-life for the precursor-treated TiO<sub>2</sub> electrodes was in good

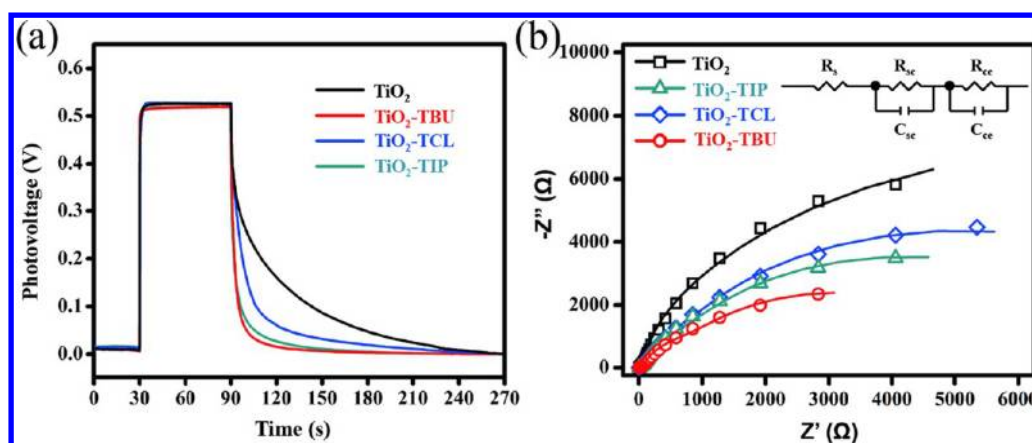


**Figure 4.** (a) Photovoltage–time spectra collected for pristine  $\text{TiO}_2$ ,  $\text{TiO}_2$ -TCL,  $\text{TiO}_2$ -TIP, and  $\text{TiO}_2$ -TBU nanowire electrodes. (b) EIS spectra of pristine  $\text{TiO}_2$ ,  $\text{TiO}_2$ -TCL,  $\text{TiO}_2$ -TIP, and  $\text{TiO}_2$ -TBU nanowire electrodes. Inset shows the equivalent circuit used to fit the spectra.

**Table 1. Equivalent Circuit-Fitting Results and Kinetic Analysis for Pristine  $\text{TiO}_2$ ,  $\text{TiO}_2$ -TCL,  $\text{TiO}_2$ -TIP, and  $\text{TiO}_2$ -TBU Nanowire Electrodes**

	$R_s$ ( $\Omega$ )	$R_{sc}$ ( $\Omega$ )	$C_{sc}$ (F)	$R_{ce}$ ( $\Omega$ )	$C_{ce}$ (F)	$\tau_c$ (ms)
$\text{TiO}_2$	97	$13.5 \times 10^3$	$1.3 \times 10^{-3}$	$8.8 \times 10^2$	$1.7 \times 10^{-3}$	58.8
$\text{TiO}_2$ -TCL	95	$8.6 \times 10^3$	$1.9 \times 10^{-3}$	$8.3 \times 10^2$	$1.5 \times 10^{-3}$	61.6
$\text{TiO}_2$ -TIP	90	$6.9 \times 10^3$	$2.2 \times 10^{-3}$	$8.1 \times 10^2$	$2.1 \times 10^{-3}$	65.9
$\text{TiO}_2$ -TBU	100	$4.6 \times 10^3$	$2.5 \times 10^{-3}$	$8.5 \times 10^2$	$1.5 \times 10^{-3}$	87.0

agreement with their IPCE results. Therefore, the photovoltage decay results supported that the enhanced photoactivity of the precursor-treated  $\text{TiO}_2$  electrodes in PEC water splitting can be attributed to the passivation of surface trap states.

Furthermore, EIS serves as a powerful method for the study of charge transfer at the semiconductor/electrolyte interface.<sup>42</sup> We performed EIS measurements to investigate the influence of A- $\text{TiO}_2$  shell coating on the interfacial charge carrier dynamics of the  $\text{TiO}_2$  photoanodes. Figure 4b shows the Nyquist plots of the PEC cells fabricated with pristine  $\text{TiO}_2$  and precursor-treated  $\text{TiO}_2$  nanowire electrodes. The impedance spectra were strongly affected by the precursor-treatment, indicating that the deposition of A- $\text{TiO}_2$  layer has changed the charge transfer at the electrode/electrolyte interface. The equivalent circuit<sup>43</sup> used to fit the EIS data was depicted in the inset of Figure 4b. In the model,  $R_s$  is the series resistance, which includes the sheet resistance of the FTO substrate and the external contact resistance of the cell. The parallel elements,  $R_{sc}$ ,  $C_{sc}$ ,  $R_{ce}$ , and  $C_{ce}$ , characterize the charge transfer resistance and the double layer capacitance for the  $\text{TiO}_2$  electrode and Pt counter electrode. The fitted data for these elements are summarized in Table 1. As shown in Table 1,  $R_{sc}$  of the  $\text{TiO}_2$  nanowire electrodes decreased after precursor-treatment. The reduction of  $R_{sc}$  indicated that the charge transfer became more efficient at the  $\text{TiO}_2$ /electrolyte interface as a result of the effective passivation of the surface trap states. Among the three types of precursor-treated  $\text{TiO}_2$  electrodes, the  $\text{TiO}_2$ -TBU electrode showed the smallest  $R_{sc}$ , suggesting that the TBU-treatment led to the most effective surface passivation for  $\text{TiO}_2$  nanowires. This conclusion was again consistent with the trend observed in IPCE enhancement. Furthermore, the diffusion–recombination model was used for analyzing the EIS spectra, which could estimate the lifetime of charge transfer at the interface ( $\tau_c$ ).<sup>9</sup> The characteristic time  $\tau_c$  also reflects the carrier lifetime for the tested electrode. The calculated  $\tau_c$  values for the pristine  $\text{TiO}_2$  and precursor-treated  $\text{TiO}_2$  nanowire electrodes

in PEC cells were compared in Table 1. All precursor-treated  $\text{TiO}_2$  electrodes exhibit a longer  $\tau_c$  than the pristine  $\text{TiO}_2$  electrode, which demonstrated that the precursor-treatment operation can extend the carrier lifetime of  $\text{TiO}_2$  nanowires. The longest  $\tau_c$  observed for the  $\text{TiO}_2$ -TBU electrode corresponded well with the results of IPCE and photovoltage measurements, in which  $\text{TiO}_2$ -TBU exhibited the most significantly enhanced photoactivity among all the precursor-treated  $\text{TiO}_2$  electrodes. These results also indicate that the photoanode performance is closely related to the precursor used for forming the A- $\text{TiO}_2$  passivation layer. The  $\text{TiCl}_4$ -treatment generated a highly rough surface of  $\text{TiO}_2$  nanowire, which could induce a high density of structural defects, causing charge recombination to shorten the carrier lifetime as observed. On the other hand, the superiority of TBU-treatment over TIP-treatment in PEC performance enhancement for  $\text{TiO}_2$  nanowires could be attributed to the reactivity difference between the two precursors. Both TBU and TIP are typical titanium alkoxides precursor used in sol–gel synthesis of  $\text{TiO}_2$  colloids. It has been reported that the hydrolysis and condensation rates of titanium alkoxides can be reduced as the size of alkoxy groups increases, which resulted in the formation of small colloidal clusters with more uniform size.<sup>44,45</sup> Since TBU has relatively larger alkoxy groups than TIP, slower hydrolysis and condensation processes are expected for the TBU-treatment, thus resulting in the slower nucleation and growth rates of the A- $\text{TiO}_2$ . The slow A- $\text{TiO}_2$  deposition could relieve the formation of lattice strain at the R- $\text{TiO}_2$ /A- $\text{TiO}_2$  interface, which explains why  $\text{TiO}_2$ -TBU electrode exhibited longer carrier lifetime and enhanced PEC performance compared to  $\text{TiO}_2$ -TIP.

Furthermore, the enhanced photocurrent could also be reasoned as due to the increased surface area and/or the improved light-harvesting of  $\text{TiO}_2$  as a result of formation of the additional A- $\text{TiO}_2$  shell. To determine the effect of A- $\text{TiO}_2$  shell on surface area and light absorption of  $\text{TiO}_2$  photoanode,

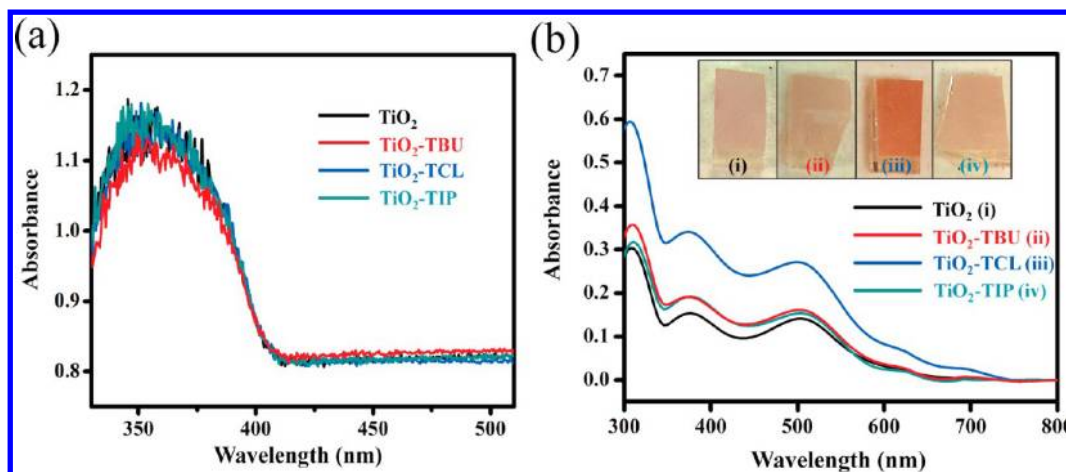


**Figure 5.** (a) Absorption spectra for pristine  $\text{TiO}_2$  and precursor-treated  $\text{TiO}_2$  nanowire array films. (b) Absorption spectra for the N3-adsorbed samples after they were immersed in a base solution for N3 desorption. Inset shows the corresponding apparent color of the samples.

the absorption spectra of the pristine  $\text{TiO}_2$  and precursor-treated  $\text{TiO}_2$  electrodes were collected to assess the light-harvesting ability of  $\text{TiO}_2$ . Figure 5a displays the corresponding UV–visible spectra of the samples, which showed an electronic transition from the valence band to the conduction band of  $\text{TiO}_2$  in the UV region. Obviously, the light-harvesting ability of the  $\text{TiO}_2$  nanowire electrode was not altered after the precursor-treatment operation. This observation ruled out the possible contribution from the increase of photon harvesting of  $\text{TiO}_2$  upon the precursor-treatment operation. Moreover, it may also be argued that the surface area of the precursor-treated  $\text{TiO}_2$  nanowires might have changed to account for the resultant PEC performance enhancement. To address this concern, an adsorption–desorption experiment by using N3 as the indicator dye was performed. Note that N3 dye is commonly used as a sensitizer for the  $\text{TiO}_2$  electrode in the fabrication of DSSCs because its COOH functional group can adsorb onto the surface of the  $\text{TiO}_2$  photoelectrode.<sup>46</sup> Desorption of N3 dye can easily occur when the N3-adsorbed  $\text{TiO}_2$  electrode is immersed in a basic solution, which can be utilized to estimate the apparent surface area of a  $\text{TiO}_2$  electrodes.<sup>31</sup> Figure 5b presents the UV–visible spectra for the samples after they were adsorbed by N3 and then immersed in an ethanolic solution containing NaOH. The N3-adsorption capacity of pristine  $\text{TiO}_2$ ,  $\text{TiO}_2$ -TIP, and  $\text{TiO}_2$ -TBU electrodes was similar, while  $\text{TiO}_2$ -TCL exhibited higher N3 adsorption ability, which can be identified from the apparent color difference of the electrodes shown in the inset of Figure 5b. The number of adsorbed molecules ( $\text{mol}/\text{cm}^2$ ) of N3 on pristine  $\text{TiO}_2$  and precursor-treated  $\text{TiO}_2$  nanowire electrodes can be further interpreted through the calibration absorption curve of the N3 dye. The adsorbed N3 dye on pristine  $\text{TiO}_2$ ,  $\text{TiO}_2$ -TCL,  $\text{TiO}_2$ -TIP, and  $\text{TiO}_2$ -TBU electrodes were 0.039, 0.081, 0.043, and 0.045  $\text{mol}/\text{cm}^2$ , respectively. This result signified that the apparent surface areas of the  $\text{TiO}_2$ -TIP and  $\text{TiO}_2$ -TBU electrodes were equivalent to that of the pristine  $\text{TiO}_2$  electrode, while the  $\text{TiO}_2$ -TCL electrode with rough surface had approximately twice the surface area of the pristine  $\text{TiO}_2$ . This phenomenon further supported that the improved PEC performance of the  $\text{TiO}_2$ -TIP and  $\text{TiO}_2$ -TBU electrodes was related to effective surface passivation rather than an increase in surface area. As for the  $\text{TiO}_2$ -TCL electrode, the improved PEC performance could be partly ascribed to the

surface area effect because the increase in surface area was evident.

## CONCLUSION

In summary, we have demonstrated a facile, yet effective, precursor-treatment method to greatly improve the PEC properties of  $\text{TiO}_2$  nanowires. Among the different precursor-treated  $\text{TiO}_2$  nanowires,  $\text{TiO}_2$ -TBU showed the most significantly enhanced photoactivity and long-term stability in PEC water oxidation. The results of IPCE measurements showed that the photocurrent enhancement was mainly due to the improved photoactivity of  $\text{TiO}_2$  in the UV region. The photovoltage and EIS results proved that the enhanced photoactivity of precursor-treated  $\text{TiO}_2$  nanowires resulted from the effective passivation of the surface states, which suppressed trap state-mediated charge recombination to facilitate the interfacial charge transfer as well as improve the overall carrier utilization efficiency. The present precursor-treatment approach could be extended to other metal oxide electrodes for achieving effective surface passivation to enhance the overall carrier utilization efficiency. This wet-chemistry-based passivation method is economically favorable for the massive production of highly photoactive  $\text{TiO}_2$  electrodes.

## ASSOCIATED CONTENT

### Supporting Information

XRD and Raman spectra; voltammograms and optimal precursor amounts for enhancing the photocurrent density of  $\text{TiO}_2$  nanowire electrode; HR-TEM image of thick A- $\text{TiO}_2$  layer coated  $\text{TiO}_2$  nanowire sample. This material is available free of charge via the Internet at <http://pubs.acs.org>.

## AUTHOR INFORMATION

### Corresponding Authors

\*Y.-J.H.: e-mail, [yhsu@cc.nctu.edu.tw](mailto:yhsu@cc.nctu.edu.tw).

\*Y.L.: e-mail, [yli@chemistry.ucsc.edu](mailto:yli@chemistry.ucsc.edu).

### Notes

The authors declare no competing financial interest.

## ACKNOWLEDGMENTS

Y.-J.H. acknowledges financial support from the National Science Council of Taiwan (Grants NSC-102-3113-P-009-002 and NSC-102-2113-M-009-005-MY2). Y.-C.P. thanks the

National Science Council of Taiwan for sponsoring the Graduate Students Study Abroad Program (Grant NSC-102-2917-I-009-042). J.Z.Z. is grateful to the BES Division of the U.S. DOE for financial support.

## REFERENCES

- (1) Walter, M. G.; Warren, E. L.; McKone, J. R.; Boettcher, S. W.; Santori, Q.; Mi, E. A.; Lewis, N. S. Solar Water Splitting Cells. *Chem. Rev.* **2010**, *110*, 6446–6473.
- (2) Kudo, A.; Miseki, Y. Heterogeneous Photocatalyst Materials for Water Splitting. *Chem. Soc. Rev.* **2009**, *38*, 253–278.
- (3) Lin, Y.; Yuan, G.; Liu, R.; Zhou, S.; Sheehan, S. W.; Wang, D. Semiconductor Nanostructure-Based Photoelectrochemical Water Splitting: A Brief Review. *Chem. Phys. Lett.* **2011**, *507*, 209–215.
- (4) Liu, C.; Dasgupta, N. P.; Yang, P. Semiconductor Nanowires for Artificial Photosynthesis. *Chem. Mater.* **2014**, *26*, 415–422.
- (5) Fujishima, A.; Honda, K. Electrochemical Photolysis of Water at a Semiconductor Electrode. *Nature* **1972**, *238*, 37–38.
- (6) Wang, G.; Wang, H.; Ling, Y.; Tang, Y.; Yang, X.; Fitzmorris, R. C.; Wang, C.; Zhang, J. Z.; Li, Y. Hydrogen-Treated TiO<sub>2</sub> Nanowire Arrays for Photoelectrochemical Water Splitting. *Nano Lett.* **2011**, *11*, 3026–3033.
- (7) Mohapatra, S. K.; Misra, M.; Mahajan, V. K.; Raja, K. S. Design of a Highly Efficient Photoelectrolytic Cell for Hydrogen Generation by Water Splitting: Application of TiO<sub>2-x</sub>C<sub>x</sub> Nanotubes as a Photoanode and Pt/TiO<sub>2</sub> Nanotubes as a Cathode. *J. Phys. Chem. C* **2007**, *111*, 8677–8685.
- (8) Cho, I. S.; Chen, Z.; Forman, A. J.; Kim, D. R.; Rao, P. M.; Jaramillo, T. F.; Zheng, X. Branched TiO<sub>2</sub> Nanorods for Photoelectrochemical Hydrogen Production. *Nano Lett.* **2011**, *11*, 4978–4984.
- (9) Yang, J.-S.; Liao, W.-P.; Wu, J.-J. Morphology and Interfacial Energetics Controls for Hierarchical Anatase/Rutile TiO<sub>2</sub> Nanostructured Array for Efficient Photoelectrochemical Water Splitting. *ACS Appl. Mater. Interfaces* **2013**, *5*, 7425–7431.
- (10) Wolcott, A.; Smith, W. A.; Kuykendall, T. R.; Zhao, Y.; Zhang, J. Z. Photoelectrochemical Water Splitting Using Dense and Aligned TiO<sub>2</sub> Nanorod Arrays. *Small* **2009**, *5*, 104–111.
- (11) Shankar, K.; Basham, J. I.; Allam, N. K.; Varghese, O. K.; Mor, G. K.; Feng, X.; Paulose, M.; Seabold, J. A.; Choi, K.-S.; Grimes, C. A. Recent Advances in the Use of TiO<sub>2</sub> Nanotube and Nanowire Arrays for Oxidative Photoelectrochemistry. *J. Phys. Chem. C* **2009**, *113*, 6327–6359.
- (12) Noh, S. Y.; Sun, K.; Choi, C.; Niu, M.; Yang, M.; Xu, K.; Jin, S.; Wang, D. Branched TiO<sub>2</sub>/Si Nanostructures for Enhanced Photoelectrochemical Water Splitting. *Nano Energy* **2013**, *2*, 351–360.
- (13) Palmas, S.; Polcaro, A. M.; Ruiz, J. R.; Pozzo, A. D.; Mascia, M.; Vacca, A. TiO<sub>2</sub> Photoanodes for Electrically Enhanced Water Splitting. *Int. J. Hydrogen Energy* **2010**, *35*, 6561–6570.
- (14) Jiang, Z.; Tang, Y.; Tay, Q.; Zhang, Y.; Malyi, O. I.; Wang, D.; Deng, J.; Lai, Y.; Zhou, H.; Chen, X.; Dong, Z.; Chen, Z. Understanding the Role of Nanostructures for Efficient Hydrogen Generation on Immobilized Photocatalysts. *Adv. Energy Mater.* **2013**, *3*, 1368–1380.
- (15) Xie, M.; Fu, X.; Jing, L.; Luan, P.; Feng, Y.; Fu, H. Long-Lived, Visible-Light-Excited Charge Carriers of TiO<sub>2</sub>/BiVO<sub>4</sub> Nanocomposites and Their Unexpected Photoactivity for Water Splitting. *Adv. Energy Mater.*, **2014**, Issue 5 (Apr 2), DOI: 10.1002/aenm.201300995.
- (16) Tang, J.; Kong, B.; Wang, Y.; Xu, M.; Wang, Y.; Wu, H.; Zheng, G. Photoelectrochemical Detection of Glutathione by IrO<sub>2</sub>-Hemin-TiO<sub>2</sub> Nanowire Arrays. *Nano Lett.* **2013**, *13*, 5350–5354.
- (17) Grätzel, M. Photoelectrochemical Cells. *Nature* **2001**, *414*, 338–344.
- (18) Leng, W. H.; Zhang, Z.; Zhang, J. Q.; Cao, C. N. Investigation of the Kinetics of a TiO<sub>2</sub> Photoelectrocatalytic Reaction Involving Charge Transfer and Recombination through Surface States by Electrochemical Impedance Spectroscopy. *J. Phys. Chem. B* **2005**, *109*, 15008–15023.
- (19) Liu, M.; Snapp, N. d. L.; Park, H. Water Photolysis with a Cross-Linked Titanium Dioxide Nanowire Anode. *Chem. Sci.* **2011**, *2*, 80–87.
- (20) van de Krol, R.; Liang, Y.; Schoonman, J. Solar Hydrogen Production with Nanostructured Metal Oxides. *J. Mater. Chem.* **2008**, *18*, 2311–2320.
- (21) Kargar, A.; Sun, K.; Jing, Y.; Choi, C.; Jeong, H.; Jung, G. Y.; Jin, S.; Wang, D. 3D Branched Nanowire Photoelectrochemical Electrodes for Efficient Solar Water Splitting. *ACS Nano* **2013**, *7*, 9407–9415.
- (22) Feng, X.; Shankar, K.; Varghese, O. K.; Paulose, M.; Latempa, T. J.; Grimes, C. A. Vertically Aligned Single Crystal TiO<sub>2</sub> Nanowire Arrays Grown Directly on Transparent Conducting Oxide Coated Glass: Synthesis Details and Applications. *Nano Lett.* **2008**, *8*, 3781–3786.
- (23) Feng, X.; Zhu, K.; Frank, A. J.; Grimes, C. A.; Mallouk, T. E. Rapid Charge Transport in Dye-Sensitized Solar Cells Made from Vertically Aligned Single-Crystal Rutile TiO<sub>2</sub> Nanowires. *Angew. Chem., Int. Ed.* **2012**, *51*, 2727–2730.
- (24) Hwang, Y. J.; Hahn, C.; Liu, B.; Yang, P. Photoelectrochemical Properties of TiO<sub>2</sub> Nanowire Arrays: A Study of the Dependence on Length and Atomic Layer Deposition Coating. *ACS Nano* **2012**, *6*, 5060–5069.
- (25) Paracchino, A.; Laporte, V.; Sivula, K.; Grätzel, M.; Thimsen, E. Highly Active Oxide Photocathode for Photoelectrochemical Water Reduction. *Nat. Mater.* **2011**, *10*, 456–461.
- (26) Lin, Y.; Xu, Y.; Mayer, M. T.; Simpson, Z. I.; McMahon, G.; Zhou, S.; Wang, D. Growth of p-Type Hematite by Atomic Layer Deposition and Its Utilization for Improved Solar Water Splitting. *J. Am. Chem. Soc.* **2012**, *134*, 5508–5511.
- (27) Mali, S. S.; Betty, C. A.; Bhosale, P. N.; Patil, P. S. Hydrothermal Synthesis of Rutile TiO<sub>2</sub> with Hierarchical Microspheres and Their Characterization. *CrystEngComm* **2011**, *13*, 6349–6351.
- (28) Hosono, E.; Fujihara, S.; Kakiuchi, K.; Imai, H. Growth of Submicrometer-Scale Rectangular Parallelepiped Rutile TiO<sub>2</sub> Films in Aqueous TiCl<sub>3</sub> Solutions under Hydrothermal Conditions. *J. Am. Chem. Soc.* **2004**, *126*, 7790–7791.
- (29) Huang, Q.; Gao, L. A Simple Route for the Synthesis of Rutile TiO<sub>2</sub> Nanorods. *Chem. Lett.* **2003**, *32*, 638–639.
- (30) Liu, L.; Qian, J.; Li, B.; Cui, Y.; Zhou, X.; Guo, X.; Ding, W. Fabrication of Rutile TiO<sub>2</sub> Tapered Nanotubes with Rectangular Cross-Sections via Anisotropic Corrosion Route. *Chem. Commun.* **2010**, *46*, 2402–2404.
- (31) Lv, M.; Zheng, D.; Ye, M.; Sun, L.; Xiao, J.; Guo, W.; Lin, C. Densely Aligned Rutile TiO<sub>2</sub> Nanorod Arrays with High Surface Area for Efficient Dye-Sensitized Solar Cells. *Nanoscale* **2012**, *4*, 5872–5879.
- (32) Wang, Y.; Zhang, Y.-Y.; Tang, J.; Wu, H.; Xu, M.; Peng, Z.; Gong, X.-G.; Zheng, G. Simultaneous Etching and Doping of TiO<sub>2</sub> Nanowire Arrays for Enhanced Photoelectrochemical Performance. *ACS Nano* **2013**, *7*, 9375–9383.
- (33) Cho, I. S.; Logar, M.; Lee, C. H.; Cai, L.; Prinz, F. B.; Zheng, X. Rapid and Controllable Flame Reduction of TiO<sub>2</sub> Nanowires for Enhanced Solar Water-Splitting. *Nano Lett.* **2014**, *14*, 24–31.
- (34) Wang, H.; Wang, G.; Ling, Y.; Lepert, M.; Wang, C.; Zhang, J. Z.; Li, Y. Photoelectrochemical Study of Oxygen Deficient TiO<sub>2</sub> Nanowire Arrays with CdS Quantum Dot Sensitization. *Nanoscale* **2012**, *4*, 1463–1466.
- (35) Pesci, F. M.; Wang, G.; Klug, D. R.; Li, Y.; Cowan, A. J. Efficient Suppression of Electron–Hole Recombination in Oxygen-Deficient Hydrogen-Treated TiO<sub>2</sub> Nanowires for Photoelectrochemical Water Splitting. *J. Phys. Chem. C* **2013**, *117*, 25837–25844.
- (36) Wang, G.; Ling, Y.; Li, Y. Oxygen-Deficient Metal Oxide Nanostructures for Photoelectrochemical Water Oxidation and Other Applications. *Nanoscale* **2012**, *4*, 6682–6691.
- (37) Stroyuk, A. L.; Kryukov, A. I.; Kuchmiy, S. Y.; Pokhodenko, V. D. Quantum Size Effects in Semiconductor Photocatalysis. *Theor. Exp. Chem.* **2005**, *41*, 207–228.
- (38) Dresselhaus, G. Effective Mass Approximation for Excitons. *J. Phys. Chem. Solids* **1956**, *1*, 15–23.



- (39) Enright, B.; Fitzmaurice, D. Spectroscopic Determination of Electron and Hole Effective Masses in a Nanocrystalline Semiconductor Film. *J. Phys. Chem.* **1996**, *100*, 1027–1035.
- (40) Pu, Y.-C.; Wang, G.; Chang, K.-D.; Ling, Y.; Lin, Y.-K.; Fitzmorris, B. C.; Liu, C.-M.; Lu, X.; Tong, Y.; Zhang, J. Z.; Hsu, Y.-J.; Li, Y. Au Nanostructure-Decorated TiO<sub>2</sub> Nanowires Exhibiting Photoactivity across Entire UV–Visible Region for Photoelectrochemical Water Splitting. *Nano Lett.* **2013**, *13*, 3817–3823.
- (41) Mukherjee, B.; Wilson, W.; Subramanian, V. R. TiO<sub>2</sub> Nanotube (T\_NT) Surface Treatment Revisited: Implications of ZnO, TiCl<sub>4</sub>, and H<sub>2</sub>O<sub>2</sub> Treatment on the Photoelectrochemical Properties of T\_NT and T\_NT–CdSe. *Nanoscale* **2013**, *5*, 269–274.
- (42) Bertoluzzi, L.; Bisquert, J. Equivalent Circuit of Electrons and Holes in Thin Semiconductor Films for Photoelectrochemical Water Splitting Applications. *J. Phys. Chem. Lett.* **2012**, *3*, 2517–2522.
- (43) Lopes, T.; Andrade, L.; Ribeiro, H. A.; Mendes, A. Characterization of Photoelectrochemical Cells for Water Splitting by Electrochemical Impedance Spectroscopy. *Int. J. Hydrogen Energy* **2010**, *35*, 11601–11608.
- (44) Livage, J.; Henry, M.; Sanchez, C. Sol–Gel Chemistry of Transition Metal Oxides. *Prog. Solid State Chem.* **1988**, *18*, 259–341.
- (45) Wang, C.-C.; Ying, J. Y. Sol–Gel Synthesis and Hydrothermal Processing of Anatase and Rutile Titania Nanocrystals. *Chem. Mater.* **1999**, *11*, 3113–3120.
- (46) Ling, Y.; Cooper, J. K.; Yang, Y.; Wang, G.; Munoz, L.; Wang, H.; Zhang, J. Z.; Li, Y. Chemically Modified Titanium Oxide Nanostructures for Dye-Sensitized Solar Cells. *Nano Energy* **2013**, *2*, 1373–1382.